Eur. Phys. J. A **24**, 13–22 (2005)
DOI 10.1140/epja/i2004-10116-7

THE EUROPEAN PHYSICAL JOURNAL A

# Collective structures of the $^{131}$Cs nucleus

R. Kumar[1], Kuljeet Singh[1], D. Mehta[1], Nirmal Singh[1,a], S.S. Malik[2], E.S. Paul[3], A. Görgen[4,b], S. Chmel[4], R.P. Singh[5], and S. Muralithar[5]

[1] Department of Physics, Panjab University, Chandigarh 160 014, India
[2] Department of Physics, Guru Nanak Dev University, Amritsar 143 005, India
[3] Oliver Lodge Laboratory, University of Liverpool, L69 7ZE, UK
[4] Helmholtz-Institut für Strahlen- und Kernphysik, Universität Bonn, Nußallee 14-16, D-53115 Bonn, Germany
[5] Nuclear Science Centre, Aruna Asaf Ali Marg, New Delhi 110 067, India

Received: 6 September 2004 / Revised version: 7 December 2004 /
Published online: 17 January 2005 – 
Communicated by D. Schwalm

**Abstract.** The collective structures of $^{131}$Cs have been investigated by in-beam $\gamma$-ray spectroscopic techniques following the $^{124}$Sn ($^{11}$B, 4n) reaction at a beam energy $E_{\rm lab} = 57$ MeV. The previously established rotational bands, built on $\pi g_{7/2}$, $\pi d_{5/2}$ and the unique-parity $\pi h_{11/2}$ orbitals, have been extended and evolve into new bands involving rotationally aligned $\nu(h_{11/2})^2$ and $\pi(h_{11/2})^2$ quasiparticles. In addition, a new multiquasiparticle band based on the $\pi g_{7/2} \otimes \nu g_{7/2} \otimes \nu h_{11/2}$ configuration has also been observed. Theoretical interpretations for the assigned configurations are discussed in the framework of Total Routhian Surface (TRS) and Tilted Axis Cranking (TAC) model calculations. TAC model calculations predict a decrease in the $B(M1)$ values with increasing rotational frequency for the $\pi g_{7/2}/\pi d_{5/2} \otimes \nu(h_{11/2})^2$ and $\pi h_{11/2} \otimes \nu(h_{11/2})^2$ bands, thus indicating a magnetic rotation character for these bands.

**PACS.** 21.10.Re Collective levels – 23.20.Lv $\gamma$ transitions and level energies – 21.60.-n Nuclear structure models and methods – 27.60.+j $90 \leq A \leq 149$

## 1 Introduction

The nuclear shape in the $A \sim 130$ mass region is characterized by a core soft with respect to the triaxiality coordinate ($\gamma$) and is regulated by the various occupied orbitals at the nuclear Fermi surface. Theoretical calculations predict a variety of minima in the nuclear potential energy surface, and indeed low-deformation minima are found experimentally to coexist with oblate, triaxial or highly deformed minima [1,2]. In recent years, structures generated by rotation of the deformed triaxial nuclei about a tilted axis, *viz.*, chirality [3] and magnetic rotation [4], have been the focus of attention. Chirality is related to the breaking of left-right symmetry in the intrinsic system of triaxial nuclei and magnetic rotation is related to the breaking of rotational symmetry by the current-distribution in nearly spherical nuclei. The $_{55}$Cs nuclei are expected to display a rich variety of band structures as the deformation remains well developed across a large range of the neutron Fermi surface. The $\pi h_{11/2} \otimes \nu h_{11/2}$ bands in the doubly odd $^{124-132}$Cs isotopes have been good candidates to study chirality [5]. A magnetic dipole band based on the $\pi h_{11/2} \otimes \nu(d_{5/2}) \otimes \nu(h_{11/2})^2$ configuration has been reported in the doubly odd $^{132}$Cs nucleus [6,7]. Recent observations of chiral bands in the odd-$A$ $^{135}$Nd [8] and even-even $^{136}$Nd [9] nuclei, and the dipole bands observed in this mass region [10] incite further investigations in the odd-$A$ $_{55}$Cs nuclei. The purpose of the present work is to investigate structural features of the $^{131}$Cs nucleus. Excited states in $^{131}$Cs have previously been studied by Garg *et al.* [11] via $^{124}$Sn ($^{10}$B, 3n) and $^{128}$Te ($^{6}$Li, 3n) reactions. The level structure, consisting of sequences built on the $\pi h_{11/2}$ and $\pi g_{7/2}$ orbitals, was reported up to $I \sim 25/2\hbar$. The low-lying states in $^{131}$Cs have been studied following the electron-capture decay of $^{131}$Ba [12]. The $5/2^+$ state ($T_{1/2}$ = 9.69 days) has been established as the ground state.

## 2 Experimental techniques and data analysis

In the present work, the $^{124}$Sn ($^{11}$B, 4n) reaction at a beam energy of 57 MeV was used to populate excited states in the $^{131}$Cs nucleus. The $^{11}$B beam was provided by the 15UD pelletron accelerator at the Nuclear Science Centre, New Delhi. The target consisted of a 3 mg/cm$^2$ thick

[a] e-mail: nsingh@pu.ac.in
[b] Present address: DAPNIA/SPhN, CEA Saclay, F-91191 Gif-sur-Yvette, France.

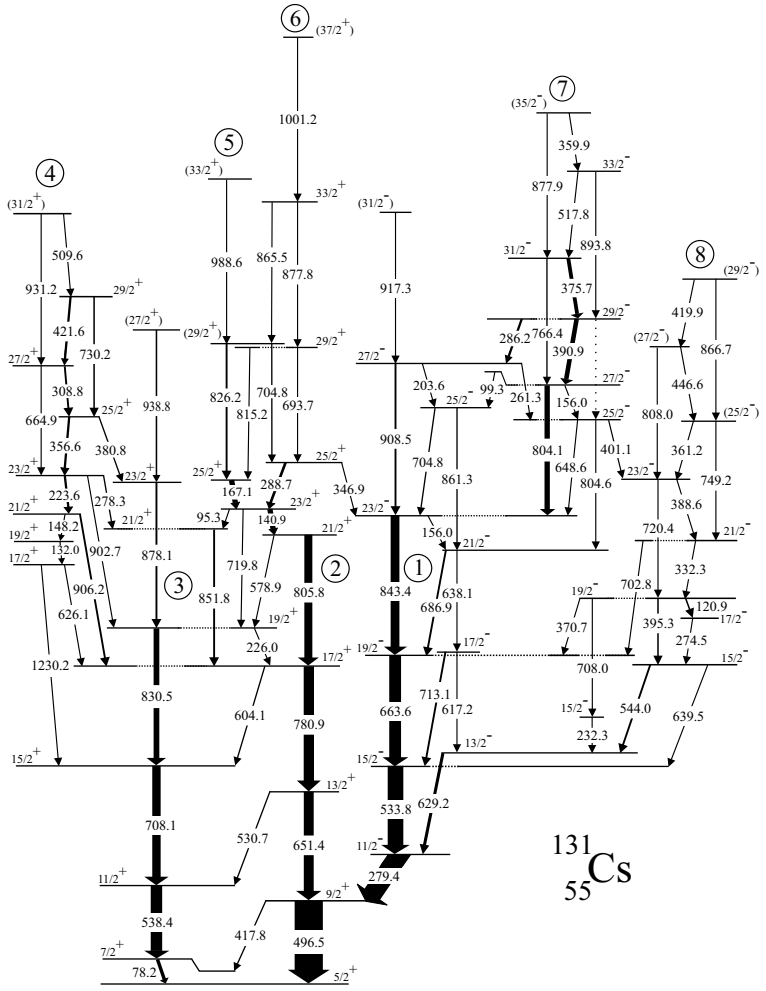


**Fig. 1.** The level scheme of $^{131}$Cs established from the present work.

isotopically enriched $^{124}$Sn foil rolled onto a 20 mg/cm$^2$ natural Pb backing. The gamma rays emitted by the evaporation residues were detected using the Gamma Detector Array (GDA). The array comprised 12 Compton-suppressed Ge detectors and a 14-element BGO multiplicity filter. The Ge detectors were mounted in three groups of four each making angles of 45°, 99° and 153° with the beam direction and having an inclination of ±23° with the horizontal plane. The multiplicity filter consisted of two sets of seven closely packed hexagonal BGO elements (size = 3.8 × 7.5 cm long), mounted above and below the target chamber. The online data were written in LIST mode for events in which two or more Ge detectors fired in prompt coincidence with two or more elements of the multiplicity filter (fold $K \geq 2$). A coincidence time window of $2\tau = 200$ ns was used and a total of $2 \times 10^8$ Ge-Ge coincidence events were collected in this experiment. The major nuclei populated in the reaction were $^{129}$Cs (4%), $^{130}$Cs (35%) and $^{131}$Cs (45%). In the offline analysis, the coincidence events were sorted into $4k \times 4k$ $E_\gamma$-$E_\gamma$ matrices with different conditions and were used to i) establish coincidence and intensity relationships for various gamma transitions and ii) perform an angular correlation analysis using the method of directional correlation from oriented states (DCO) [13] for characterizing the dipole/quadrupole nature of the gamma transitions. Background-subtracted coincidence spectra were generated and intensity analysis was performed using the computer codes GATESET [14] and PEAKFIT [15], respectively.

The present level scheme of $^{131}$Cs, based on the ground state ($T_{1/2} = 9.688$ d) with $I^\pi = 5/2^+$, is shown in fig. 1, where the band structures have been labelled 1-8 to facilitate the discussion. The placement of the gamma transitions in the level scheme is based upon their intensities, energy sums and coincidence relationships. Representative coincidence gamma-ray spectra depicting transitions of the new bands along with the connecting transitions to the earlier known levels [11] are shown in figs. 2(a)-(d). The properties of the gamma rays assigned to $^{131}$Cs together with their placement in the level scheme are listed in table 1. The spin-parity assignments for band 4 are based upon the quadrupole ($E2$) nature of the 906.2 keV ($21/2^+ \rightarrow 17/2^+$) and the dipole (taken to be $M1$) nature of the 380.8 keV ($25/2^+ \rightarrow 23/2^+$) interband transitions. Band 7 is assigned negative parity on the basis

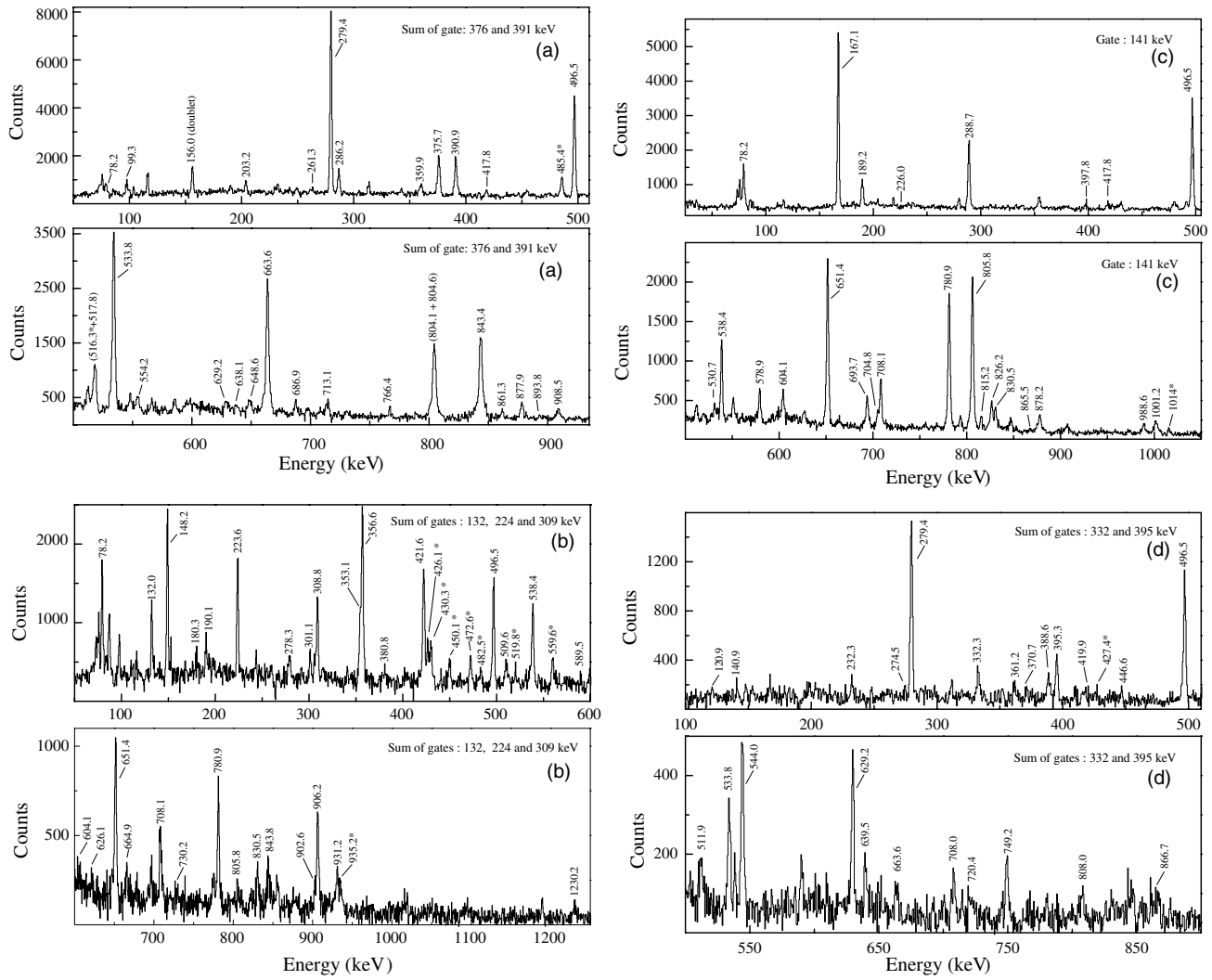


**Fig. 2.** Gamma ray coincidence spectra with gates on various transitions of $^{131}$Cs. The peaks labelled with (∗) belong to $^{131}$Cs, but their placement in the level scheme is not ascertained. The unmarked peaks are contaminants.

of the quadrupole ($E2$) nature of the 804.1 keV transition ($27/2^- \rightarrow 23/2^-$). The spin-parity for band 8 is assigned on the basis of the 544.0 keV ($15/2^- \rightarrow 13/2^-$), 332.3 keV ($21/2^- \rightarrow 19/2^-$) and 232.3 keV ($15/2^- \rightarrow 13/2^-$) dipole transitions (taken as $M1$) and the 395.3 keV quadrupole ($E2$) transition ($19/2^- \rightarrow 15/2^-$). Further, negative parity for this band is also supported from its decay to the negative-parity band 1. The gamma transitions corresponding to peaks marked * in fig. 2(b) lie above the $(29/2^+)$ level of band 4. However, the exact placement of these transitions could not be ascertained.

The earlier known level scheme of $^{131}$Cs [11] has been substantially extended up to $I = 37/2\hbar$ with the addition of about seventy new transitions. The level scheme inferred from the present work preserves major features of the previously observed bands 1, 2 and 3, which have been assigned to be based on the $\pi h_{11/2}$, $\pi d_{5/2}$ and $\pi g_{7/2}$ orbitals, respectively. The positive-parity band 4 and negative-parity band 7 comprise strong dipole transitions along with weak $E2$ crossover transitions. In the coupled band 8, intensities of the $M1$ transitions are of the order of those for the stretched $E2$ crossover transitions. Bands 5 and 6 consist of $E2$ transitions and also have interlinking $E2$ transitions. The decay patterns of bands 4-8 are quite complex, mostly connecting to the low-lying states with either negative or positive parity.

## 3 Results and discussion

The level scheme of $^{131}$Cs shows properties typical of a collectively rotating deformed nucleus. Nilsson configuration assignments to various observed bands are based on arguments concerning the band-crossing frequencies, signature splitting, additivity of alignments of the involved quasiparticles and the deduced $B(M1)/B(E2)$ ratios. The experimentally determined spins and level energies have been transformed into the rotating frame of reference following the prescription of Bengtsson and Frauendorf [16]. The Harris parameters [17], $J_0 = 5.8\,\hbar^2\,\mathrm{MeV}^{-1}$

**Table 1.** Gamma-ray energies, intensities, DCO ratios and multipolarities for transitions assigned to $^{131}$Cs.

| $E$ (keV)[a] | Intensity[b] | DCO ratio | Assigned multipolarity | Placement $I_i^\pi \to I_f^\pi$ |
|---|---|---|---|---|
| 78.2 | 102 | | $M1$[c] | $7/2^+ \to 5/2^+$ |
| 95.3 | 15 | | $(M1)$ | $23/2^+ \to 21/2^+$ |
| 99.3 | 5 | | $(M1)$ | $27/2^- \to 25/2^-$ |
| 120.9 | 5 | | $(M1)$ | $19/2^- \to 17/2^-$ |
| 132.0 | 19 | 0.71 (15) | $M1$ | $19/2^+ \to 17/2^+$ |
| 140.9 | 182 | 0.69 (7) | $M1$ | $23/2^+ \to 21/2^+$ |
| 148.2 | 20 | 0.64 (15) | $M1$ | $21/2^+ \to 19/2^+$ |
| 156.0 | 11 | 0.38 (12) | $M1$ | $27/2^- \to 25/2^-$ |
| 156.0 | 19 | 0.38 (10) | $M1$ | $23/2^- \to 21/2^-$ |
| 167.1 | 143 | 0.54 (5) | $M1$ | $25/2^+ \to 23/2^+$ |
| 203.2 | 34 | 0.64 (10) | $M1$ | $27/2^- \to 25/2^-$ |
| 223.6 | 74 | 0.59 (7) | $M1$ | $23/2^+ \to 21/2^+$ |
| 226.6 | 5 | | $(M1)$ | $19/2^+ \to 17/2^+$ |
| 232.3 | 28 | 0.65 (9) | $M1$ | $15/2^- \to 13/2^-$ |
| 261.3 | 13 | | $(M1)$ | $27/2^- \to 25/2^-$ |
| 274.5 | 18 | 0.58 (11) | $M1$ | $17/2^- \to 15/2^-$ |
| 278.3 | 22 | | $(M1)$ | $23/2^+ \to 21/2^+$ |
| 279.4 | 671 | 0.61 (4) | $E1$ | $11/2^- \to 9/2^+$ |
| 286.2 | 76 | 0.57 (7) | $M1$ | $29/2^- \to 27/2^-$ |
| 288.7 | 96 | 0.49 (11) | $M1$ | $25/2^+ \to 23/2^+$ |
| 308.8 | 67 | 0.53 (7) | $M1$ | $27/2^+ \to 25/2^+$ |
| 332.3 | 36 | 0.64 (10) | $M1$ | $21/2^- \to 19/2^-$ |
| 346.9 | 16 | | $(E1)$ | $25/2^+ \to 23/2^-$ |
| 356.6 | 76 | 0.50 (7) | $M1$ | $25/2^+ \to 23/2^+$ |
| 359.9 | 27 | | $(M1)$ | $(35/2^-) \to 33/2^-$ |
| 361.2 | 23 | | $(M1)$ | $(25/2^- \to 23/2^-)$ |
| 370.7 | 12 | | $(M1)$ | $19/2^- \to 19/2^-$ |
| 375.7 | 142 | 0.42 (5) | $M1$ | $31/2^- \to 29/2^-$ |
| 380.8 | 15 | 0.39 (10) | $M1$ | $25/2^+ \to 23/2^+$ |
| 388.6 | 27 | | $(M1)$ | $23/2^- \to 21/2^-$ |
| 390.9 | 158 | 0.39 (8) | $M1$ | $29/2^- \to 27/2^-$ |
| 395.3 | 50 | 1.04 (12) | $E2$ | $19/2^- \to 15/2^-$ |
| 401.1 | 5 | | $(M1)$ | $25/2^- \to 23/2^-$ |
| 417.8 | 51 | | $(M1)$ | $9/2^+ \to 7/2^+$ |
| 419.9 | 5 | | $(M1)$ | $(29/2^-) \to (27/2^-)$ |
| 421.6 | 81 | 0.58 (7) | $M1$ | $29/2^+ \to 27/2^+$ |
| 446.6 | 12 | | $(M1)$ | $(27/2^-) \to (25/2^-)$ |
| 496.5 | 1000 | 1.05 (7) | $E2$ | $9/2^+ \to 5/2^+$ |
| 509.6 | 20 | | $(M1)$ | $(31/2^+) \to 29/2^+$ |
| 517.8 | 34 | 0.53 (9) | $M1$ | $33/2^- \to 31/2^-$ |
| 530.7 | 26 | | $(M1)$ | $13/2^+ \to 11/2^+$ |
| 533.8 | 557 | 0.88 (8) | $E2$ | $15/2^- \to 11/2^-$ |
| 538.4 | 394 | 1.02 (8) | $E2$ | $11/2^+ \to 7/2^+$ |
| 544.0 | 73 | 0.34 (9) | $M1$ | $15/2^- \to 13/2^-$ |
| 578.9 | 39 | 0.40 (9) | $M1$ | $21/2^+ \to 19/2^+$ |
| 604.1 | 55 | 0.40 (8) | $M1$ | $17/2^+ \to 15/2^+$ |
| 617.2 | 23 | | $(E2)$ | $17/2^- \to 13/2^-$ |
| 626.1 | 22 | | | $17/2^+ \to 17/2^+$ |
| 629.2 | 111 | 0.40 (6) | $M1$ | $13/2^- \to 11/2^-$ |
| 638.1 | 16 | | $(E2)$ | $21/2^- \to 17/2^-$ |
| 639.5 | 19 | | $(M1)$ | $15/2^- \to 15/2^-$ |
| 648.6 | 43 | 0.58 (9) | $M1$ | $25/2^- \to 23/2^-$ |
| 651.4 | 353 | 0.88 (7) | $E2$ | $13/2^+ \to 9/2^+$ |
| 663.6 | 426 | 1.10 (8) | $E2$ | $19/2^- \to 15/2^-$ |
| 664.9 | 22 | | $(E2)$ | $27/2^+ \to 23/2^+$ |
| 686.9 | 65 | 0.38 (9) | $M1$ | $21/2^- \to 19/2^-$ |
| 693.7 | 44 | 0.84 (15) | $(E2)$ | $(29/2^+) \to 25/2^+$ |

**Table 1.** Continued.

| $E$ (keV)[a] | Intensity[b] | DCO ratio | Assigned multipolarity | Placement $I_i^\pi \to I_f^\pi$ |
|---|---|---|---|---|
| 702.8 | 15 | | $(M1)$ | $21/2^- \to 19/2^-$ |
| 704.8 | 16 | | $(M1)$ | $25/2^- \to 23/2^-$ |
| 704.8 | 19 | | $(E2)$ | $(29/2^+) \to 25/2^+$ |
| 708.0 | 17 | | $(E2)$ | $19/2^- \to 15/2^-$ |
| 708.1 | 304 | 0.87 (8) | $E2$ | $15/2^+ \to 11/2^+$ |
| 713.1 | 74 | 0.44 (8) | $M1$ | $17/2^- \to 15/2^-$ |
| 719.8 | 35 | 1.03 (18) | $E2$ | $23/2^+ \to 19/2^+$ |
| 720.4 | 19 | | $(E2)$ | $23/2^- \to 19/2^-$ |
| 730.2 | 16 | | $(E2)$ | $29/2^+ \to 25/2^+$ |
| 749.2 | 35 | | $(E2)$ | $(25/2^-) \to 21/2^-$ |
| 766.4 | 40 | 0.88 (16) | $E2$ | $31/2^- \to 27/2^-$ |
| 780.9 | 369 | 1.13 (11) | $E2$ | $17/2^+ \to 13/2^+$ |
| 804.1 | 190 | 1.23 (12) | $E2$ | $27/2^- \to 23/2^-$ |
| 804.6 | 7 | | | $25/2^- \to 21/2^-$ |
| 805.8 | 277 | 0.97 (8) | $E2$ | $21/2^+ \to 17/2^+$ |
| 808.0 | 45 | | $(E2)$ | $(27/2^-) \to 23/2^-$ |
| 815.2 | 30 | | $(E2)$ | $(29/2^+) \to 25/2^+$ |
| 826.2 | 65 | | $(E2)$ | $(29/2^+) \to 25/2^+$ |
| 830.5 | 209 | 0.89 (12) | $E2$ | $19/2^+ \to 15/2^+$ |
| 843.4 | 319 | 0.84 (12) | $E2$ | $23/2^- \to 19/2^-$ |
| 851.8 | 65 | | $(E2)$ | $21/2^+ \to 17/2^+$ |
| 861.3 | 54 | | $(E2)$ | $25/2^- \to 21/2^-$ |
| 865.5 | 20 | | $(E2)$ | $(33/2^+) \to (29/2^+)$ |
| 866.7 | 23 | | $(E2)$ | $(29/2^-) \to (25/2^-)$ |
| 877.8 | 44 | 0.83 (17) | $E2$ | $33/2^+ \to 29/2^+$ |
| 877.9 | 39 | | $(E2)$ | $(35/2^-) \to 31/2^-$ |
| 878.1 | 75 | 0.86 (17) | $E2$ | $23/2^+ \to 19/2^+$ |
| 893.8 | 7 | | $(E2)$ | $33/2^- \to 29/2^-$ |
| 902.7 | 30 | | $(E2)$ | $23/2^+ \to 19/2^+$ |
| 906.2 | 65 | 1.03 (15) | $E2$ | $21/2^+ \to 17/2^+$ |
| 908.5 | 66 | 0.82 (15) | $E2$ | $27/2^- \to 23/2^-$ |
| 917.3 | 13 | | $(E2)$ | $(31/2^-) \to 27/2^-$ |
| 931.2 | 30 | | $(E2)$ | $(31/2^+) \to 27/2^+$ |
| 938.8 | 17 | | $(E2)$ | $(27/2^+) \to 23/2^+$ |
| 988.6 | 38 | | $(E2)$ | $(33/2^+) \to (29/2^+)$ |
| 1001.2 | 47 | | $(E2)$ | $(37/2^+) \to 33/2^+$ |
| 1230.2 | 12 | | $(M1)$ | $17/2^+ \to 15/2^+$ |

(a) Energies are accurate to 0.3 keV for strong transitions. The errors increase to 0.7 keV for weaker transitions (relative intensity < 30).
(b) Errors in $\gamma$-ray intensities are 5–20%.
(c) Assigned multipolarity adopted from the earlier work [11].

and $J_1 = 50.8\,\hbar^4\,\mathrm{MeV}^{-3}$, have been used. The Routhian ($e'$) and alignment ($i_x$) extracted for different bands are shown as a function of rotational frequency in fig. 3. The experimental ratios of reduced transition probabilities, $B(M1; I \to I-1)/B(E2; I \to I-2)$ in units of $(\mu_\mathrm{N}/\mathrm{eb})^2$, for the coupled bands 4, 7 and 8 are deduced from the relation

$$\frac{B(M1; I \to I-1)}{B(E2; I \to I-2)} = 0.697 \frac{I_\gamma(M1)}{I_\gamma(E2)} \frac{E_\gamma^5(E2)}{E_\gamma^3(M1)}, \quad (1)$$

where $E_\gamma$ is the energy of the gamma ray in MeV. The $E2/M1$ mixing ratio ($\delta$) for the $\Delta I = 1$ transition has been set to zero. This assumption does not influence the experimental results since the mixing ratio is generally small. The experimental $B(M1)/B(E2)$ values are compared with theoretical calculations obtained from the semiclassical model of Dönau and Frauendorf [18,19]. The rotational gyromagnetic factor ($g_R$) was taken as $Z/A = 0.42$ and empirical values of the gyromagnetic factors ($g_i$) of the participating quasiparticles, taken from nearby nuclei [20], were used. The quadrupole moment ($Q_0$) values deduced corresponding to the deformation parameter ($\beta_2$) as obtained from the TRS calculations (discussed later in this section), have been used.

The negative-parity sequence built on the $11/2^-$ state is the favoured (signature $\alpha = -1/2$) partner in the $\pi h_{11/2}$ band (band 1) and the weakly populated sequence comprising of the 617, 638 and 861 keV transitions is the unfavoured ($\alpha = +1/2$) one. The $\Delta I = 1$ transitions linking the two signature partners are also observed and the

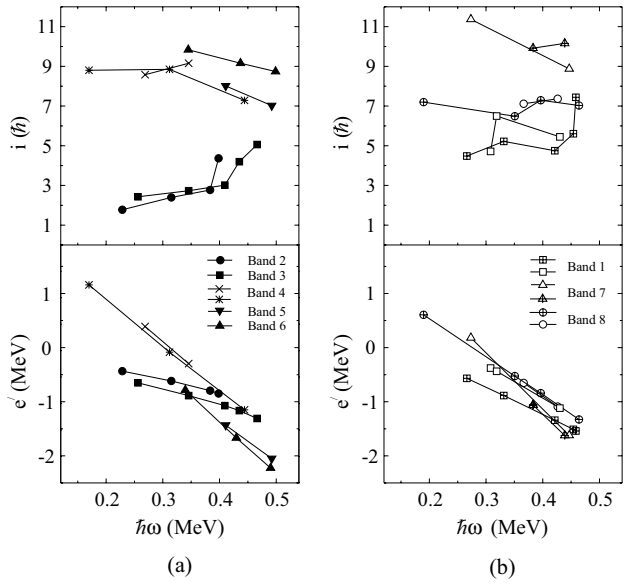


**Fig. 3.** Experimental Routhian and alignment plots for the bands 1-8 observed in $^{131}$Cs.

staggering pattern which depends upon the triaxiality coordinate ($\gamma$) is similar to that observed in the $^{125,127,129}$Cs [21] isotopes. The band shows large initial alignment ($\sim 5\hbar$) and signature splitting ($\Delta e' \sim 390\,\mathrm{keV}$ at $\hbar\omega = 0.30\,\mathrm{MeV}$) exhibiting a trend decreasing with frequency (fig. 3(b)). The low-$\Omega$ $h_{11/2}[550]1/2^-$ orbital, which is near to the proton Fermi surface accounts for these features. A small upbend is observed in the favoured signature partner at a rotational frequency of $\hbar\omega \sim 0.45\,\mathrm{MeV}$ (fig. 3(b)), which could be the onset of the decoupling of a $\pi h_{11/2}$ pair. The first proton crossing, expected at $\sim 0.38\,\mathrm{MeV}$ [22], is Pauli-blocked and the second one is predicted to occur above 0.50 MeV. Band 1 is crossed by band 7 at a rotational frequency of $\hbar\omega \sim 0.42\,\mathrm{MeV}$ with a corresponding gain in alignment $\sim 5\hbar$ (fig. 3(b)). This crossing in band 1 is interpreted as the rotational alignment of a $\nu h_{11/2}$ pair in accordance with the systematics of that observed in the $\pi h_{11/2}$ band in the odd-mass $^{117-129}$Cs isotopes [23]. Thus, band 7 is assigned the $\pi h_{11/2} \otimes (\nu h_{11/2})^2$ configuration. The magnitude of the signature splitting in the aligned band 7 is reduced to $\sim 90\,\mathrm{keV}$ from a value $\sim 390\,\mathrm{keV}$ in the prolate $\pi h_{11/2}$ band (band 1). This can be explained on the basis of cranking shell model calculations, which predict that the aligning $\nu(h_{11/2})^2$ pair drives the core towards the collectively rotating oblate ($\gamma \approx -60^\circ$ (Lund convention [24])) shape (fig. 9 of [25]). However, a significant signature splitting ($\sim 90\,\mathrm{keV}$) in band 7 indicates that the neutron polarizing effect has resulted in a weakly triaxial shape. The large values of the experimental $B(M1; I \rightarrow I-1)/B(E2; I \rightarrow I-2)$ ratios $\sim 14$ $(\mu_\mathrm{N}/\mathrm{eb})^2$ in band 7 agree with the value $\sim 12$ $(\mu_\mathrm{N}/\mathrm{eb})^2$ calculated using the geometrical model of Dönau and Frauendorf [18,19] for the assigned configuration. The $\gamma$-vibrational band built on the favoured signature partner of $h_{11/2}$ band, a feature observed in the $^{123,125,127}$Cs isotopes [25–27], is not observed in the heavier $^{129,131,133}$Cs isotopes [11,28].

The evenly spaced positive-parity bands 2 and 3 built on the $5/2^+$ and the $7/2^+$ states have been assigned the $\pi d_{5/2}$ and $\pi g_{7/2}$ [11] configurations, respectively. These bands are populated with nearly equal strengths, despite the fact that the Routhian for band 2 is $\sim 170\,\mathrm{keV}$ above that of band 3 (fig. 3(a)). This rules out the possibility of these bands being signature partners. Weak intraband dipole transitions from the $\pi d_{5/2}$ band to the $\pi g_{7/2}$ band are observed. Similar sequences have also been observed in the $_{55}$Cs [25–29] and $_{53}$I [30,31] nuclei. The $\pi h_{11/2}$ and $\pi g_{7/2}$ bands are seen in the odd-$A$ $^{117,121-133}$Cs isotopes [11,23,25–29]. The population strength of the $\pi g_{7/2}$ band relative to that of the $\pi h_{11/2}$ band increases considerably with increasing mass number. This happens primarily because the excitation energy of the $h_{11/2}$ level is increasing thus becoming less yrast in the heavier isotopes. Also, the coupled band based on the $\pi g_{9/2}[404]9/2^+$ orbital is seen in the lighter odd-$A$ $^{117-127}$Cs [23,25–27,29] isotopes but is not observed in $^{129,131}$Cs [28]. These facts are consistent with a decreasing nuclear deformation with increasing mass.

The positive-parity band 4 comprises mainly strong $\Delta I = 1$ dipole transitions and decays into levels of the $\pi d_{5/2}$ (band 2) and $\pi g_{7/2}$ (band 3) bands. This band is characterized by a large constant alignment $\sim 9\hbar$ and small signature splitting $\sim 30\,\mathrm{keV}$ (fig. 3(a)). Band 4 crosses bands 2 and 3 at a rotational frequency $\sim 0.45\,\mathrm{MeV}$ with a corresponding alignment gain $\sim 6\hbar$, which suggests a $(\nu h_{11/2})^2$ alignment similar to the one observed for band 1 (fig. 3(b)). A multi-quasiparticle $\pi g_{7/2}/d_{5/2} \otimes (\nu h_{11/2})^2$ configuration is thus suggested for this band. The signature splitting $\sim 30\,\mathrm{keV}$ in this band is smaller as compared to $\sim 90\,\mathrm{keV}$ in band 7, which is understandable as the $\pi g_{7/2}$ orbital is lesser prolate driving as compared to the $\pi h_{11/2}$ orbital, and hence can counteract the oblate driving effect of the aligned $(\nu h_{11/2})^2$ to a lesser extent. The deduced values of the $B(M1; I \rightarrow I-1)/B(E2; I \rightarrow I-2)$ ratios for the $27/2^+$ and $29/2^+$ levels are $\sim 10$ $(\mu_\mathrm{n}/\mathrm{eb})^2$. It decreases to $\sim 3$ $(\mu_\mathrm{N}/\mathrm{eb})^2$ at the $31/2^+$ level. It is worth mentioning that the crossover $E2$ transitions (664.9 and 730.2 keV) are observed only in the higher part of the band 4. This indicates a decreasing trend for the $B(M1)/B(E2)$ values with frequency. These characteristics are similar to that of the observed $M1$ bands in the $A \sim 130$ and $A \sim 190$ regions [4]. The decreasing trend of the $B(M1)/B(E2)$ ratios, which is likely due to a decrease in the $B(M1)$ values, is a feature related to magnetic rotation.

Bands 5 and 6 exhibit large alignment $\sim 9\hbar$ (fig. 3(a)) indicating that these are essentially based on three-quasiparticle configurations and are continuations of one-quasiparticle bands 2 and 3. The closely lying Routhians and the $E2$ transitions interlinking the bands 5 and 6 indicate these to be based on similar configurations. Large alignment gain $\sim 7.5\hbar$ in bands 5 and 6 indicates low-$\Omega$ $(\pi h_{11/2})^2$ alignment, which is also possible in the bands 2 and 3 apart from the $\nu(h_{11/2})^2$ alignment and is expected at $\hbar\omega \sim 0.4\,\mathrm{MeV}$. Bands 5 and 6 cross bands 2 and 3 at similar frequencies (fig. 3(a)), hence,

**Table 2.** Average TRS quadrupole deformation parameters calculated for $^{131}$Cs.

| Band | Configuration | $\beta_2$ | $\beta_4$ | $\gamma$ |
|---|---|---|---|---|
| 1 | $E(h_{11/2})$ | 0.157 | 0.003 | 35° |
| 1 | $F(h_{11/2})$ | 0.157 | 0.003 | −33° |
| 2 | $A(d_{5/2})$ | 0.127 | −0.007 | 32° |
| 3 | $B(g_{7/2})$ | 0.125 | −0.008 | 21° |
| 4 | $Bef$ | 0.142 | −0.008 | −85° |
| 5 | $BEF$ | 0.161 | 0.000 | 35° |
| 6 | $AEF$ | 0.165 | 0.002 | 35° |
| 7 | $Eef$ | 0.160 | 0.001 | −82° |
| 8 | $Bbe$ | 0.145 | −0.010 | −85° |

$\pi d_{5/2}/g_{7/2} \otimes \pi(h_{11/2})^2$ are the likely configurations suggested for these bands. Such $\pi(h_{11/2})^2$ alignments have also been observed as decoupled bands for the odd-$A$ $^{125-127}$La isotopes [32,33] in contrast to the coupled bands after the $\nu(h_{11/2})^2$ alignment.

The negative-parity coupled band 8 shows a large initial alignment $\sim 7\hbar$ and a small signature splitting $\Delta e' \sim 20$ keV at $\hbar\omega = 0.36$ MeV (fig. 3(b)). The experimental $B(M1)/B(E2)$ ratios for this band are $\sim 2$ $(\mu_N/\text{eb})^2$. This band is believed to be built on a mixed proton-neutron three-quasiparticle configuration. For such a configuration in an odd-$Z$ nucleus, a high-$K$ two-quasineutron configuration would be coupled to the odd quasiproton. Since the negative-parity strongly coupled bands based on the $\nu g_{7/2} \otimes \nu h_{11/2}$ configuration have systematically been observed in the even-even $^{124-128}$Xe [34–37] and $^{124-128}$Ba isotopes [38–40], and the $\pi g_{7/2}$ orbital is lowest in energy in case of $^{131}$Cs, the most likely choice for band 8 is the negative-parity $\pi g_{7/2} \otimes \nu g_{7/2} \otimes \nu h_{11/2}$ configuration. Strongly coupled bands based on the $\pi g_{7/2} \otimes \nu g_{7/2} \otimes \nu h_{11/2}$ configuration are also observed in the neighbouring $^{125,127}$Cs isotopes [25,27]. These bands include the high-$\Omega$ $[404]7/2^+$ neutron orbital, from the top of the $\nu g_{7/2}$ shell, which is responsible for strong $\Delta I = 1$ transitions and small signature splitting. It is added that the other likely configuration $\pi g_{7/2} \otimes \nu d_{5/2} \otimes \nu h_{11/2}$ is not preferred for band 8 as the $B(M1)/B(E2)$ values $\sim 5$ $(\mu_N/\text{eb})^2$ calculated using the geometrical model of Dönau and Frauendorf [18,19] are significantly higher. The calculated values for the $\pi g_{7/2} \otimes \nu h_{11/2} \otimes \nu g_{7/2}$ configurations exhibit good agreement.

### 3.1 Theoretical model calculations

Calculations based on the Total Routhian Surface (TRS) formalism [41–43] have been performed for $^{131}$Cs. These calculations employed a triaxial Woods-Saxon single-particle potential [44] and a monopole pairing force residual interaction. Self-consistent deformation parameters $\beta_2$, $\beta_4$ and $\gamma$ for different quasiparticle configurations were evaluated for different values of the rotational frequency. The results show that this nucleus is extremely $\gamma$-soft. Three energy minima occur for values of the triaxiality parameter $\gamma$ close to +30°, −30°, and −90°. These

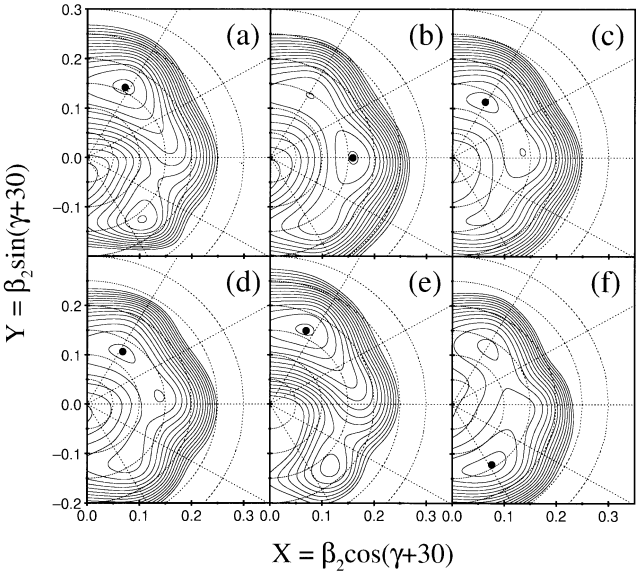


**Fig. 4.** TRS maps for (a) $E$, (b) $F$, (c) $A$, (d) $B$, (e) $AEF$ and (f) $Bbe$ configurations in $^{131}$Cs. The energy contours are separated by 150 keV.

special values represent the same nuclear shape; the nucleus is just rotating about different axes, *i.e.* short, intermediate, or long. It is found that different occupied single-quasiparticle orbitals stabilize the overall nuclear shape near these three minima. For instance, proton orbitals from the bottom of the negative-parity $h_{11/2}$ or positive-parity $g_{7/2}$ and $d_{5/2}$ orbitals drive towards the $\gamma = +30°$ shape, while neutron orbitals from the top of the $\nu h_{11/2}$ subshell drive towards the $\gamma = -90°$ shape. Results for different configurations are summarized in table 2, which were calculated at $\hbar\omega = 0.24$ MeV; TRS maps are also plotted in fig. 4. The single-quasiparticle levels are labelled using the parity and signature notation as: $A = \pi(+,+1/2)$, $B = \pi(+,-1/2)$, $E = \pi(-,-1/2)$, $F = \pi(-,+1/2)$, $a = \nu(+,+1/2)$, $b = \nu(+,-1/2)$, $e = \nu(-,-1/2)$, $f = \nu(-,+1/2)$. It can be seen from table 2 that the occupation of an $h_{11/2}$ quasiproton orbital drives to larger quadrupole deformation ($\beta_2$). The favoured signature $E$ strongly drives to positive $\gamma$. However, its signature partner $F$ is extremely flat with $\gamma$ and the nucleus adopts the most collective shape at $\gamma = -30°$. The positive-parity proton orbitals $A$ and $B$ also drive to positive $\gamma$, while $h_{11/2}$ neutrons ($e$ and $f$ orbitals) prefer the $\gamma = -90°$ shape.

Bands 5 and 6 are essentially three-quasiparticle continuations of one-quasiparticle bands 2 and 3. There is quite an increase in quadrupole deformation associated with the $(\pi h_{11/2})^2$ alignment (EF), which explains why the band structures are not so smooth around spin $25/2^-$. The TRS calculations suggest that the three $\Delta I = 1$ bands, *viz.* band 4, 7 and 8 have triaxial shapes close to $\gamma = -90°$ and since the proton and neutron spins are expected to be near perpendicular at the bandheads, it is appropriate to describe these bands within the shears mechanism. Hence calculations have been performed using the

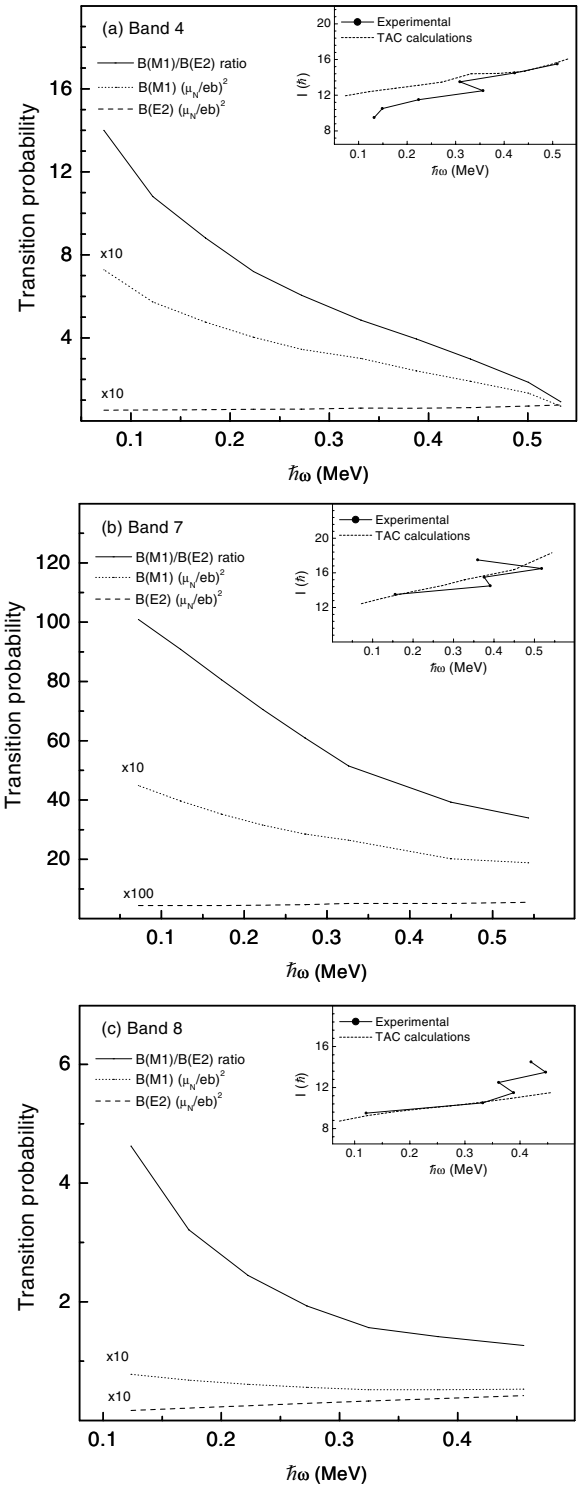


**Fig. 5.** The $M1$ and $E2$ transition probabilities and their ratios *vs.* rotational frequency ($\hbar\omega$) predicted using TAC model calculations for (a) band 4, (b) band 7 and (c) band 8. The insets show plot of the calculated (TAC) and experimental angular momentum ($I$) *vs.* rotational frequency ($\hbar\omega$).

hybrid version of the Tilted Axis Cranking (TAC) model calculations [45] for the assigned configuration. The pairing parameters are chosen as 80% of the odd-even mass difference, *i.e.*, $\Delta_\pi = 1.0796\,\text{MeV}$ and $\Delta_\nu = 0.7644\,\text{MeV}$.

The TAC model calculations [45] carried out in a self-consistent manner for band 4 with $\pi g_{7/2}(d_{5/2}) \otimes (\nu h_{11/2})^2$ configuration has resulted in the deformation parameters $\varepsilon_2 = 0.111$, $\varepsilon_4 = 0.0$, $\gamma = 46^\circ$ and an average tilt angle $\theta \sim 16^\circ$ for the angular momentum with respect to the principal axis. The results of the calculations of spin angular momentum *vs.* rotational frequency show a good agreement with the experimental values (fig. 5(a)). The calculated $B(M1)$ values exhibit a strong decreasing trend with frequency, which results in a similar trend for the corresponding $B(M1)/B(E2)$ ratios with the value dropping from $\sim 14\ (\mu_\text{N}/\text{eb})^2$ at 0.07 MeV to $\sim 6\ (\mu_\text{N}/\text{eb})^2$ at 0.27 MeV (fig. 5(a)). As mentioned earlier, the limited experimental information conforms to these predictions and band 4 is likely to be a magnetic-rotation band.

The minimization of the total energy in the TAC model calculations for band 7 with $\pi h_{11/2} \otimes (\nu h_{11/2})^2$ configuration resulted in the deformation parameters $\varepsilon_2 = 0.112$, $\varepsilon_4 = 0.01$, $\gamma = 55^\circ$ and an average tilt angle $\theta \sim 32^\circ$ for the angular momentum with respect to the principal axis. The calculations show a good agreement with the experimental plot of spin *vs.* rotational frequency (fig. 5(b)). The calculations result in $B(M1)/B(E2)$ values $\sim 30\ (\mu_\text{n}/\text{eb})^2$ compared to the experimental values for this band having an average $\sim 12\ (\mu_\text{n}/\text{eb})^2$. For $\pi h_{11/2} \otimes (\nu h_{11/2})^2$ configuration, the $B(M1)$ values also exhibit a decreasing trend and hence a magnetic-rotation character. For the $\pi g_{7/2} \otimes \nu h_{11/2} \otimes \nu g_{7/2}$ configuration assigned to band 8, TAC calculations result in minima corresponding to the deformation parameters $\varepsilon_2 = 0.104$, $\varepsilon_4 = 0.008$, $\gamma = 5^\circ$ and an average tilt angle $\theta \sim 46^\circ$. The angular value of this tilt drives the system towards triaxiality. The calculated $B(M1)/B(E2)$ values are $\sim 1.5\ (\mu_\text{n}/\text{eb})^2$ compared to the experimental value $\sim 2\ (\mu_\text{n}/\text{eb})^2$ for this band in the observed frequency region (fig. 5(c)).

## 4 Conclusion

Collective structures of the $^{131}$Cs nucleus have been studied. Nilsson configurations are assigned and discussed in the framework of Total Routhian Surface (TRS) and Tilted Axis Cranking (TAC) model calculations. The existence of collective bands of both prolate and oblate shapes in $^{131}$Cs shows that this nucleus is soft with respect to $\gamma$ and its shape is strongly influenced by the excited valence quasiparticles. A new multiquasiparticle band based on the $\pi g_{7/2} \otimes \nu g_{7/2} \otimes \nu h_{11/2}$ configuration has been observed. TAC model calculations predict a decrease in the $B(M1)$ values with increasing rotational frequency for the $\pi g_{7/2}/\pi d_{5/2} \otimes \nu(h_{11/2})^2$ and $\pi h_{11/2} \otimes \nu(h_{11/2})^2$ bands in $^{131}$Cs. The limited experimental information conforms to these predictions and these bands are likely to result from magnetic rotation. Since the characteristic decrease in the $B(M1)$ values is the definitive test of the above interpretation, level lifetime measurements are desirable.

The authors are thankful to the pelletron accelerator staff of the Nuclear Science Centre, New Delhi, for their excellent

support during the experiment. Financial support from UGC, New Delhi, under the Center of Advanced Study Funds, CSIR, New Delhi and UK Engineering and Physical Sciences Research Council is acknowledged. The authors thank Drs. R. Wyss and W. Nazarewicz for providing the TRS codes.

## References

1. Y. Liang, R. Ma, E.S. Paul, N. Xu, D.B. Fossan, Phys. Rev. Lett. **64**, 29 (1990).
2. J. Dudek, K. Pomorski, N. Schunck, N. Dubray, Eur. Phys. J. A **20**, 15 (2004).
3. V.I. Dimitrov, S. Frauendorf, F. Dönau, Phys. Rev. Lett. **84**, 5732 (2000).
4. R.M. Clark, A.O. Macchiavelli, Annu. Rev. Nucl. Part. Sci. **50**, 1 (2000).
5. T. Koike, K. Starosta, C.J. Chiara, D.B. Fossan, D.R. LaFosse, Phys. Rev. C **67**, 044319 (2003).
6. G. Rainovski, E.S. Paul, H.J. Chantler, P.J. Nolan, D.G. Jenkins, R. Wadsworth, P. Raddon, A. Simons, D.B. Fossan, T. Koike, K. Starosta, C. Vaman, E. Farnea, A. Gadea, Th. Kroll, R. Isocrate, G. de Angelis, D. Curien, V.I. Dimitrov, Phys. Rev. C **68**, 024318 (2003).
7. G. Rainovski, E.S. Paul, H.J. Chantler, P.J. Nolan, D.G. Jenkins, R. Wadsworth, P. Raddon, A. Simons, D.B. Fossan, T. Koike, K. Starosta, C. Vaman, E. Farnea, A. Gadea, Th. Kroll, G. de Angelis, R. Isocrate, D. Curien, V.I. Dimitrov, J. Phys. G **29**, 2763 (2003).
8. S. Zhu, U. Garg, B.K. Nayak, S.S. Ghugre, N.S. Pattabiraman, D.B. Fossan, T. Koike, K. Starosta, C. Vaman, R.V.F. Janssens, R.S. Chakrawarthy, M. Whitehead, A.O. Macchiavelli, S. Frauendorf, Phys. Rev. Lett. **91**, 132501 (2003).
9. E. Mergel, C.M. Petrache, G. Lo Bianco, H. Hübel, J. Domscheit, D. Roßbach, G. Schönwaßer, N. Nenoff, A. Neußer, A. Görgen, F. Becker, E. Bouchez, M. Houry, A. Hürstel, Y. Le Coz, R. Lucas, Ch. Theisen, W. Korten, A. Bracco, N. Blasi, F. Camera, S. Leoni, F. Hannachi, A. Lopez-Martens, M. Rejmund, D. Gassmann, P. Reiter, P.G. Thirolf, A. Astier, N. Buforn, M. Meyer, N. Redon, O. Stezowski, Eur. Phys. J. A **15**, 417 (2002).
10. S. Lakshmi, H.C. Jain, P.K. Joshi, Amita, A.K. Jain, S.S. Malik, Phys. Rev. C **66**, 041303 (R) (2002).
11. U. Garg, T.P. Sjoreen, D.B. Fossan, Phys. Rev. C **19**, 207 (1979).
12. M. Sainath, D. Rani Rao, K. Vankataramaniah, P.C. Sood, Pramana **61**, 1157 (2003).
13. K.S. Krane, R.M. Steffen, R.M. Wheeler, Nucl. Data Tables A **11**, 351 (1973).
14. J. Singh, R. Singh, N. Singh, P.N. Trehan, in *Proceedings of DAE Symposium on Nuclear Physics, Utkal University, Bhubaneswar, India, 1993*, edited by R.K. Choudhury, A.K. Mohanty, Nucl. Phys. B (Proc. Suppl.) **36**, 406 (1993).
15. J. Singh, R. Singh, N. Singh, P.N. Trehan, in *Proceedings of DAE Symposium on Nuclear Physics, Utkal University, Bhubaneswar, India, 1994*, edited by R.K. Choudhury, A.K. Mohanty, Nucl. Phys. B (Proc. Suppl.) **37**, 455 (1994).
16. R. Bengtsson, S. Frauendorf, Nucl. Phys. A **327**, 139 (1979).
17. S.M. Harris, Phys. Rev. **138**, 509B (1965).
18. F. Dönau, S. Frauendorf, *Proceedings of the Conference On High Angular Momentum Properties of Nuclei, Oak Ridge, Tennessee, 1982*, edited by N.R. Johnson (Harwood Academic, New York, 1983), p. 143.
19. F. Dönau, Nucl. Phys. A **471**, 469 (1987).
20. M. Serris, C.T. Papadopoulos, R. Vlastou, C.A. Kalfas, S. Kossionides, N. Fotiades, S. Harissopulos, C.W. Beausang, M.J. Joyce, E.S. Paul, M.A. Bentley, S. Araddad, J. Simpson, J.F. Sharpey-Schafer, Z. Phys. A **358**, 37 (1997).
21. O. Vogel, A. Gelberg, R.V. Jolos, P. von Brentano, Nucl. Phys. A **576**, 109 (1994).
22. R. Ma, Y. Liang, E.S. Paul, N. Xu, D.B. Fossan, Phys. Rev. C **41**, 717 (1990).
23. J.F. Smith, V. Medina-Chico, C.J. Chiara, D.B. Fossan, G.J. Lane, J.M. Sears, I. Thorslund, H. Amro, C.N. Davids, R.V.F. Janssens, D. Seweryniak, I.M. Hibbert, R. Wadsworth, I.Y. Lee, A.O. Macchiavelli, Phys. Rev. C **63**, 024319 (2001).
24. G. Andersson, S.E. Larsson, G. Leander, P. Moller, S.G. Nilsson, I. Ragnarsson, S. Aberg, R. Bengtsson, J. Dudek, B. Nerlo-Pomorska, K. Pomorski, Z. Szymanski, Nucl. Phys. A **268**, 205 (1976).
25. J.R. Hughes, D.B. Fossan, D.R. LaFosse, Y. Liang, P. Vaska, M.P. Waring, Phys. Rev. C **44**, 2390 (1991).
26. K. Singh, J. Goswamy, D. Mehta, N. Singh, R.P. Singh, S. Muralithar, E.S. Paul, K.P. Singh, N. Madhavan, J.J. Das, S. Nath, A. Jhingan, P. Sughathan, R.K. Bhowmik, Eur. Phys. J. A **21**, 359 (2004).
27. Y. Liang, R. Ma, E.S. Paul, N. Xu, D.B. Fossan, Phys. Rev. C **42**, 890 (1990).
28. L. Hildingsson, W. Klamra, Th. Lindblad, F. Liden, Y. Liang, R. Ma, E.S. Paul, N. Xu, D.B. Fossan, J. Gascon, Z. Phys. A **340**, 29 (1991).
29. F. Lidén, B. Caderwall, P. Ahonen, D.W. Banes, B. Fant, J. Gascon, L. Hildingsson, A. Johnson, S. Juutinen, A. Kirwan, D.J.G. Love, S. Mitarai, J. Mukai, A.H. Nelson, J. Nyberg, J. Simpson, R. Wyss, Nucl. Phys. A **550**, 365 (1992).
30. S. Tormanen, S. Juutinen, R. Julin, A. Lampinen, E. Makela, M. Piiparinen, A. Savelius, A. Virtanen, G.B. Hagemann, Ch. Dorste, W. Karczmarczyk, T. Morek, J. Srebrny, K. Starosta, Nucl. Phys. A **613**, 282 (1997).
31. M.P. Waring, D.B. Fossan, D.R. LaFosse, H. Schnare, P. Vaska, Phys. Rev. C **49**, 1878 (1994).
32. D.J. Hartley, L.L. Riedinger, H.Q. Jin, W. Reviol, B.H. Smith, A. Galindo-Uribarri, D.G. Sarantites, D.R. LaFosse, J.N. Wilson, S.M. Mullins, Phys. Rev. C **60**, 014308 (1999).
33. R. Wadsworth, E.S. Paul, A. Astier, D. Bazzacco, A.J. Boston, N. Buforn, C.J. Chiara, D.B. Fossan, C. Fox, J. Gizon, D.G. Jenkins, N.S. Kelsall, T. Koike, D.R. LaFosse, S. Lunardi, P.J. Nolan, B.M. Nyako, C.M. Petrache, H. Scraggs, K. Starosta, J. Timar, A. Walker, A.N. Wilson, L. Zolnai, B.G. Dong, I. Ragnarsson, Phys. Rev. C **62**, 034315 (2000).
34. I. Schneider, R.S. Chakrawarthy, I. Wiedenhöver, A. Schmidt, H. Meise1, P. Petkov, A. Dewald, P. von Brentano, O. Stuch, K. Jessen, D. Weisshaar, C. Schumacher, O. Vogel, G. Sletten, B. Herskind, M. Bergström, J. Wrzesinski, Phys. Rev. C **60**, 014312 (1999).
35. V. Werner, H. Meise, I. Wiedenhöver, A. Gade, P. von Brentano, Nucl. Phys. A **692**, 451 (2001).

36. W. Lieberz, S. Freund, A. Granderath, A. Gelberg, A. Dewald, R. Reinhardt, R. Wirowski, K.O. Zell, P. von Brentano, Z. Phys. A **330**, 221 (1988).
37. T. Lonnroth, S. Vajda, O.C. Kistner, M.H. Rafailovich, Z. Phys. A **317**, 215 (1984).
38. S. Pilotte, S. Flibotte, S. Monaro, N. Nadon, D. Prévost, P. Taras, H.R. Andrews, D. Horn, V.P. Janzen, D.C. Radford, D. Ward, J.K. Johansson, J.C. Waddington, T.E. Drake, A. Galindo-Uribari, R. Wyss, Nucl. Phys. A **514**, 545 (1990).
39. D. Ward, V.P. Janzen, H.R. Andrews, D.C. Radford, G.C. Ball, D. Horn, J.C. Waddington, J.K. Johansson, F. Banville, J. Gascon, S. Monaro, N. Nadon, S. Pilotte, D. Prevost, P. Taras, R. Wyss, Nucl. Phys. A **529**, 315 (1991).
40. O. Vogel, R.S. Chakrawarthy, A. Dewald, P. Petkov, K. Jessen, J. Gableske, P. von Brentano, D. Bazzacco, A. Gizon, J. Gizon, S. Lunardi, D.R. Napoli, P. Pavan, C. Rossi-Alvarez, I. Wiedenhöver, Eur. Phys. J. A **4**, 323 (1999).
41. W. Nazarewicz, G.A. Leander, J. Dudek, Nucl. Phys. A **467**, 437 (1987).
42. R. Wyss, J. Nyberg, A. Johnson, R. Bengtsson, W. Nazarewicz, Phys. Lett. B **215**, 211 (1988).
43. W. Nazarewicz, R. Wyss, A. Johnson, Nucl. Phys. A **503**, 285 (1989).
44. W. Nazarewicz, J. Dudek, R. Bengtsson, I. Ragnarsson, Nucl. Phys. A **435**, 397 (1985).
45. V.I. Dimitrov, F. Dönau, S. Frauendorf, Phys. Rev. C **62**, 024315 (2000).